Evaluating the Performance of Microstructure Generation Algorithms for 2-d Foam-Like Representative Volume Elements

J. Alsayednoor , P. Harrison

PII: S0167-6636(16)30028-X
DOI: 10.1016/j.mechmat.2016.04.001
Reference: MECMAT 2574

To appear in: *Mechanics of Materials*

Received date: 11 August 2015
Revised date: 26 March 2016
Accepted date: 12 April 2016

Please cite this article as: J. Alsayednoor , P. Harrison , Evaluating the Performance of Microstructure Generation Algorithms for 2-d Foam-Like Representative Volume Elements, *Mechanics of Materials* (2016), doi: 10.1016/j.mechmat.2016.04.001

Evaluating the Performance of Microstructure Generation Algorithms for 2-d Foam-Like Representative Volume Elements

Alsayednoor [b]. J. and Harrison [a]. P.,

[a] School of Engineering, University of Glasgow, University Avenue, G12 8QQ Glasgow, UK

[b] INSIGNEO Institute for In-Silico Medicine, Department of Mechanical Engineering, University of Sheffield, Sir Fredrick Mappin Building, Mappin Street, Sheffield S1 3JD, UK

Corresponding Author:

Dr Philip Harrison, philip.harrison@glasgow.ac.uk, +44 0141 3304318

Keywords: anisotropy, foam, micro-macro, RVE, periodic

Abstract

This investigation evaluates various numerical algorithms; each designed to generate periodic 2-D Representative Volume Elements (RVEs) containing foam-like microstructures suitable for direct import into commercial finite element software for mechanical evaluation. The operation of each algorithm is discussed and the resulting RVEs are examined from both a mechanical and a morphological perspective. A basic Voronoi-based algorithm is found to be simple to implement but the method is shown to produce inherently anisotropic microstructures. Increasing the degree of irregularity of the microstructure reduces the anisotropy but at the cost of creating unrealistic microstructures, containing highly angular cells. A method of modifying such unrealistic microstructures using a centroidal tessellation relaxation algorithm is demonstrated, ultimately producing RVEs with relatively realistic mono-disperse microstructures. An alternative algorithm is also investigated the advantage of this algorithm is its ability to generate poly-disperse microstructures, with a controllable degree of poly-dispersity and an almost fully isotropic mechanical response.

1. Introduction

The microstructure of cellular foam is very important in determining its bulk mechanical response. The wide variety of cellular foam reflects the large diversity in the types of microstructure that can be found. Important parameters that can be used to describe the microstructure include the relative density [Gibson and Ashby, 1997], cellular area fraction, cellular morphology (open or closed) [Raj and Kerr, 2010], poly-dispersity of cell size [Kraynik et al. 2004; Jang et al. 2008; Jang et al. 2010; Kraynik, 2006; Mills, 2007] and statistical anisotropy of cellular dimensions [Jebur, 2012; Benouali et al. 2005]. In some cases, macro-scale models able to accurately model a foam's mechanical response might not yet be available due to the complexity of the material behaviour (e.g. hyperelastic transversely isotropic compressible continuum models) and if they are, it can often be a time consuming, difficult and expensive process to perform all the lab-based experiments required to determine the model parameters. This traditional macro-scale approach also provides little information on the underlying deformation mechanisms occurring

within the material's microstructure, and consequently provides limited scope for microstructural optimisation. With the increase in computational power, multi-scale modelling is becoming a powerful and increasingly relevant computational approach [Liebscher et al. 2013; Verhoosel et al. 2015], useful in optimising a material's underlying microstructure for specific applications. For example, changing relative density and microstructural anisotropy as a function of position, can optimise the structural response of a foam-based component according to anticipated loading conditions. Such microstructural optimisation is commonplace in many naturally occurring structures such as bone and wood. Nevertheless, micro to macro simulation of entire parts and components is computationally expensive, usually prohibitively so, leading many modellers to employ the concept of a Representative Volume Element (RVE) [Hill, 1963] in combination with a Periodic Boundary Condition (PBC) [Guedes and Kikuchi, 1990; Anthoine, 1995]. The aim here is to obtain a homogenised macro-response for a material's bulk behaviour from a small sample of the material.

The accuracy and practicality of computational homogenisation or any other micro-to-macro mapping technique, strongly depends on the choice of RVE. The latter should ideally be both realistic and computationally efficient, two criteria that are often at odds with one another [Kouznetsova et al. 2001; Smit et al. 1998; Swan, 1994]. The optimum size of the RVE and its level of detail are two important considerations [Alsayednoor et al. 2012]. When it comes to the level of detail within the RVE, one extreme strategy is to employ RVEs based on, for example, actual 3-D topologies, measured using techniques such as micro-CT imaging [Shan and Gokhale, 2001; Maire et al. 2003; Michailidis et al. 2011]. In this case, issues associated with strict application of the PBC have to be resolved [Youssef et al. 2005] together with problems related to identification of the distinct phases within the material. An alternative is to use numerical algorithms to automatically generate RVEs with periodic microstructures. Particulate composites, or porous materials with high relative density can be modelled in this way [Guo et al. 2014]. Nevertheless, long computation times resulting from use of the large number of continuum elements required in these simulations, remains a practical restriction to wider exploitation.

Modelling foams of low relative density, with microstructures containing narrow ribs or faces offers the opportunity to use structural elements, such as beam or shell, rather than continuum elements [Zhu et al. 2000; Korner et al. 2002; Roberts and Garboczi, 2002; Kraynik et al. 2003; Chen et al. 1999; Fazekas et al. 2002; Schmidt, 2004].

Despite the large number of prior numerical investigations that have employed digitally generated microstructures to model foams of low relative density, concerns regarding the realism and accuracy of these morphologies exist. Namely, can the numerical algorithms produce microstructures that accurately represent the diverse range of real morphologies observed in actual low-density cellular foams? A recognised method of generating representative randomised microstructures for cellular foams is through Voronoi tessellation [Voronoï, 1908] or alternatively through use of variants on this technique. Basic Voronoi tessellation [Aurenhammer, 1991; Zhu and Windle, 2002, Zhu et al. 2006] provides a fast and effective way to create beam-based finite element microstructures possessing morphologies that serve as a rough, first order approximation to those observed in several classes of polymeric and metallic, open and closed cell foams [Silva et al. 1995; Van der Burg et al. 1997; Shulmeister et al. 1998]. However, changes to the basic Voronoi algorithm can substantially alter the predicted microstructural morphologies. Altering the fundamental operation of the basic Voronoi algorithm, using for example the Laguerre-Voronoi approach, can produce even greater statistical changes [Fazekas et al.2002; Hardenacke and Hohe, 2009]. The main goal of the current investigation is to evaluate the realism of microstructures generated using these different techniques by recreating isotropic microstructural cellular morphologies. Note that in this investigation, the constitutive behaviour of the beam elements is the same throughout all simulations and is restricted to a simple linear-elastic material model in order to focus attention on the effects of the RVE microstructure rather than the material behaviour. In so doing, the investigation aims to highlight the relative advantages and disadvantages of the different microstructure generation algorithms .

2. Description of Numerical RVE Generation Algorithms

2.1 Basic Voronoi Tessellation

Voronoi tessellation is an algorithm designed to partition a given Euclidian surface into distinct regions. To do this individual seed points are positioned across the surface and the Voronoi algorithm is used to partition the surface into individual cells, separating each seed point from its neighbour with a cell wall positioned half way between the two seed points [Aurenhammer et al. 2000]. Various methods have been implemented to generate foam-like RVEs based on Voronoi tessellation. The methods tend to differ mainly in how the position of seed-points required by the Voronoi tessellation algorithm, are generated [e.g. Van der Burg et al. 1997; Grenestedt and Tanaka 1998; Silva and Gibson, 1997; Zhu et al. 2001[b]]. In this investigation, a combination of methods proposed by Zhu et al. (2001[b]) and Grenestedt and Tanaka (1998) is utilised [Alsayednoor et al. 2014]. This combined technique has been found to be computationally faster than the original method proposed by Zhu et al. (2001[b]), upon which it is based, nevertheless the resulting microstructures are very similar. In order to generate a periodic 2-D RVE using this method, first a unit square is populated with regular seed positions (the precursor seeding for a honeycomb pattern). Eq. (1) is then used to perturb these initial seed positions, by a distance, Δ, in an arbitrary direction, to produce a unit square containing an irregular distribution of seeds. Here Δ is given as,

$$\Delta = \frac{\alpha \times \delta_0}{100}, \quad \alpha \in (0,100) \tag{1}$$

where

$$\delta_0 = \sqrt{\frac{2A}{N\sqrt{3}}} \tag{2}$$

In equations (1) and (2), the parameter, α, controls the degree of irregularity of the microstructure, similar to the same parameter used by Zhu et al. (2001[a]), δ_0 is the minimum specified distance between each adjacent seed position, which is calculated from Eq. (2). A and N represent the area of the RVE and the number of seeds, respectively. ‘alpha’ can be set to values up to 100, though in practice setting alpha=50 is found to produce an isotropic RVE (the main motivation for randomising

the seed positions) and using higher values merely increases the angularity of the cells within the RVE, resulting in progressively less realistic microstructural morphologies. The 'perturbed' unit square seeding is copied nine times to create a larger square containing 3X3 identical perturbed unit square seedings. Applying a Voronoi tessellation algorithm to the resulting 3X3 structure produces a fully periodic cellular pattern within the central square, with pairs of counterpart nodes on opposing boundaries (see Fig. 1).

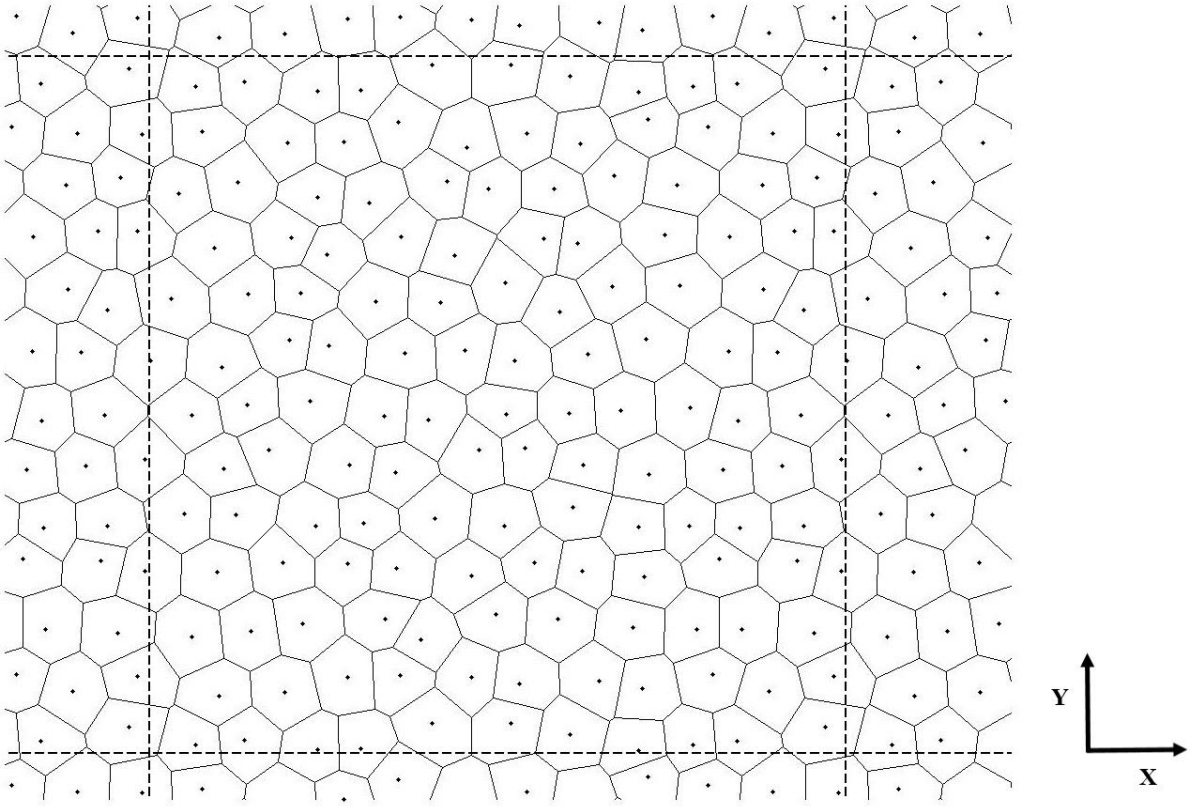

Figure 1: An example of fully periodic classical Voronoi tessellation (central square)

Later in this investigation it will be shown that the basic Voronoi method described here can introduce unwanted anisotropy in the microstructural morphology; anisotropy that is evident in the RVE's mechanical response. The same anisotropic behaviour was also observed in RVEs generated using the method proposed by Zhu et al. (2001[a]), particularly for RVEs with only low to moderate degrees of irregularity.

2.2 Centroidal Voronoi Tessellation

The Centroidal Voronoi Tessellation (CVT) algorithm can be described as an iterative 'relaxation process'. As will be shown, the CVT method is a convenient approach to removing unintended anisotropy from RVEs generated using the basic

Voronoi algorithm, producing mono-disperse digital microstructures closely resembling those of various real polymer foams. The technique runs in a reasonable computational time (less than 30 seconds when using a 64 bit Windows OS with Intel (R) Xeon (R) CPU @ 2.66 GHz and 12 GB RAM) and can be used to construct both 2-D and 3-D periodic RVEs with a highly mono-disperse cellular size distribution. This technique is a modification of the basic Voronoi method [Burkardt et al. 2002]. Liu et al. 2009 considered the Lloyd's algorithm [Lloyd, 1982] to be the best technique for computing a CVT. The algorithm can be described as an iterative 'relaxation process' where a basic Voronoi cell is generated in each iteration, though the seed position of the cell is updated at each iteration and moved towards the position of the Voronoi cell's centroid (hence the name of the algorithm), until the two eventually converge, resulting in more regular polygon containing less acute internal angles (see, for example, Fig 2).

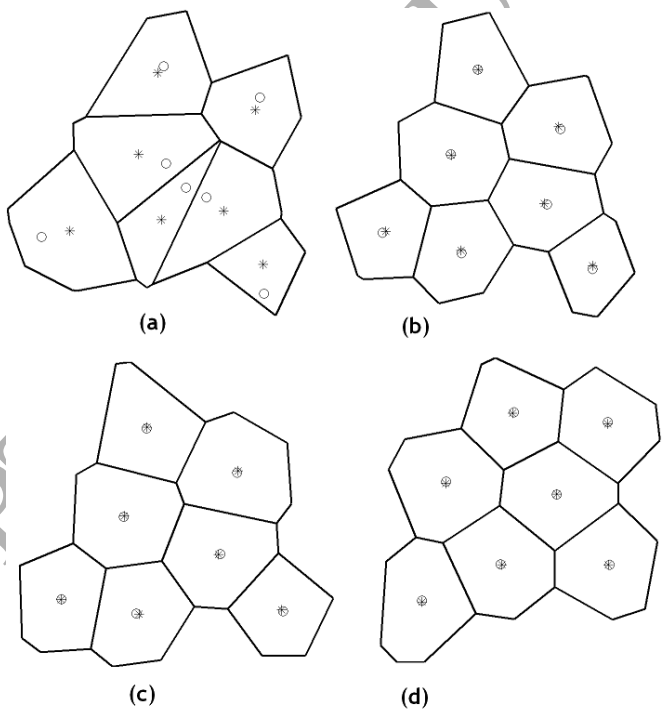

Figure 2: Illustrative example of Lloyd's algorithm. At each iteration (a, b, c, d) a centroid for each Voronoi cell is calculated (black stars) and replaced by a seed point (circles).

An example of the effect of the algorithm on the final microstructure is demonstrated in Fig 3. The figure shows the microstructure before iterative application (about 500 iterations for 500 cells) of the Lloyds relaxation algorithm. The resulting cells (Figure 3b) are of more realistic geometry and of lower poly-dispersity compared to those

generated using the basic Voronoi algorithm when employing a fully randomised seeding configuration (Figure 3a).

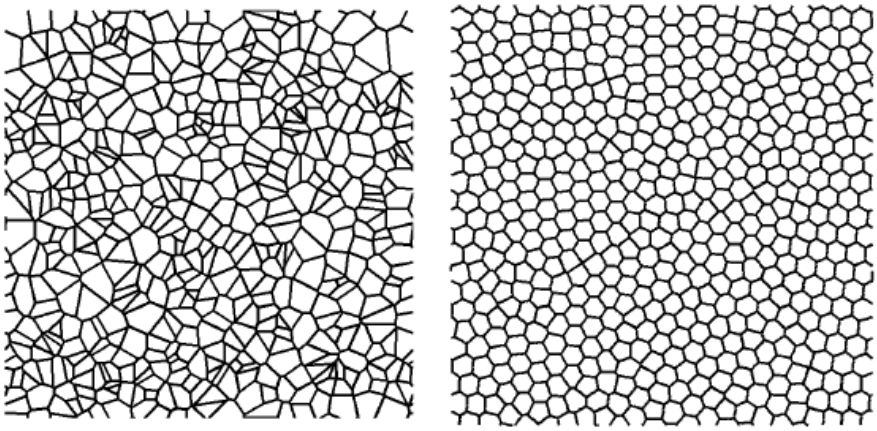

Figure 3: (a) microstructure generated by basic Voronoi technique (with α=50) before application of the relaxation algorithm and (b) the same seeding arrangement but after application of the Lloyd's algorithm.

2.3 Laguerre-Voronoi Tessellation

One important limitation of both the basic and Centroidal Voronoi Tessellation algorithms, is their inability to model poly-disperse microstructures. In general, all seed-based modelling techniques lead to symmetric Gaussian cell-size distributions [Fazekas et al.2002; Gervois et al. 2002; Kanaun and Tkachenko, 2006]. In reality, the microstructural cell-size distribution of a polydisperse foam tends more towards a log-normal or Gamma distribution [Kraynik, 2006; Montminy et al. 2004]; significantly different in form to a Gaussian distribution. To address this issue, instead of constructing Voronoi cells based on their seed point coordinates (i.e. the basic Voronoi tessellation method), each individual cell can instead be represented using a 'hard-disk' with a specified size and coordinate. Using such an approach means that cell-partitioning can be based on the location of the contact points between the hard-disks rather than the mid-way bi-sector point lying between seed positions (as is used in the basic Voronoi approach). In the Laguerre-Voronoi approach, bisectors are located at the contact point of adjacent disks rather than at the mid-way distance between their centres. The difference in the resulting microstructure is illustrated in Fig 4.

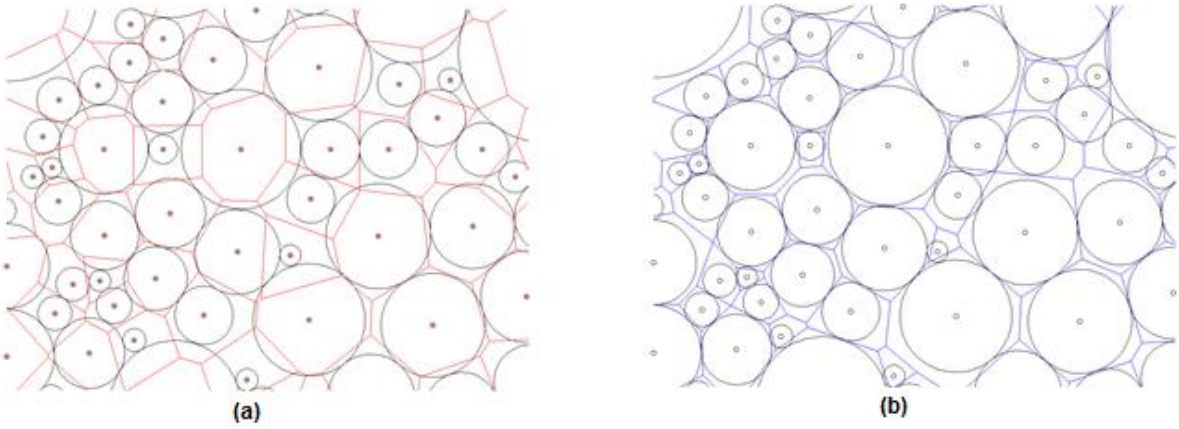

Figure 4: (a) Voronoi tessellation generated from seed positions produced by an arrangement of hard-discs (b) Laguerre Voronoi Tessellation generated using the same arrangement of hard-disks. Note the latter results in a much more polydisperse microstructure.

In general, CVT are suitable for the generation of isotropic 2-D and 3-D periodic RVEs with different degrees of irregularity, for cells with low to moderate poly-dispersity. However, for cases of large poly-dispersity, it will be shown that the Laguerre-Voronoi method is more effective. One of the main challenges of the Laguerre-Voronoi method is in creating the initial packing arrangement of hard-discs (i.e. the position and size of the non-overlapping discs shown in Figure 4). Generally, two main methods are used: (i) Random Sequential Adsorption (RSA) [Cooper, 1988] and (ii) classical hard-disk Molecular Dynamics (MD). In the RSA method, hard-disks are randomly generated with different sizes and coordinates. Random sized discs are then randomly, sequentially and irreversibly placed in the RVE, though if any overlap is detected then the disc placement is cancelled. The advantages of using RSA are its simplicity and relatively small computational resource requirement, an advantage that becomes more apparent for poly-disperse cell size distributions. Different techniques for applying the RSA method are reported in the literature; most techniques are suitable for single mode and bimodal cell size generation [Harder and Silbert, 1980; Adamczyk et al. 1997; Brilliantov et al. 1998; Rouault and Assouline, 1998; Gray et al. 2001; Richard et al. 2001; Wu et al. 2003; Gan et al. 2010]. Fan et al. [2004] applied a modified version of a collective rearrangement RSA algorithm, initially developed by He and Ekere [1998], to generate a poly-disperse polycrystalline metallic grain microstructure. In another

attempt, Farr and Groot (2009) developed a new method for packing 3-D poly-disperse spheres based on a one-dimensional mapping. Although all these approaches are applicable to both 2-D and 3-D cases, they are best suited to single or bimodal cell size distributions, a higher degree of poly-dispersity tends to be more complicated, time consuming and requires alternative algorithms. After studying most of the RSA techniques published in the literature, the Drop and Roll method was chosen for this investigation [Visscher and Bolsterli, 1972; Okubo and Odagaki, 2004]. Important advantages of the Drop and Roll method, compared to other packing algorithms, include increased contact between neighbouring disks, which results in a higher packing density, greater simplicity and a more efficient computational algorithm [Gibson, 2007]. The implementation process for generating fully periodic and relatively isotropic RVEs using a novel, modified version of the Drop and Roll method is outlined in the supplementary material.

As with the basic Voronoi technique, described in Section 2.1, when using the Drop and Roll method, a control mechanism is implemented to define the geometrical degree of irregularity of the resulting RVE. The approach used here was originally suggested by Kraynik et al. (2004) and involves generating the disk size (radius) distribution using a log-normal function, i.e.

$$\mu = In\left(\frac{m}{\sqrt{1+\frac{\gamma}{m^2}}}\right) \tag{3}$$

$$\sigma_{sd} = \sqrt{In\left(1+\frac{\gamma}{m^2}\right)} \tag{4}$$

$$r = exp\left(\mu + z\sigma_{sd}\right) \tag{5}$$

where m is the disk mean radius, γ is the variance of the disk radii, μ and σ_{sd} are the mean and standard deviation of the disk radii required to generate random data following a lognormal distribution and z is a pseudo-random variable. γ is the main parameter controlling the degree of poly-dispersity since it defines the range of disk

sizes and plays a similar role to α in the basic Voronoi method, described in Section 2.1. The 'lognrnd.m' function available in Matlab™, see Eq (5), directly calculates random values based on a log-normal frequency distribution function. Using Equations (3) and (4), with disk mean radius and variance inputs (m and γ), mean and standard deviations (μ and σ_{sd}) are calculated and used in Eq. (5). In order to avoid generation of very large or very small disks, a limit is set within a specified interval by choosing r_{min} and r_{max} for the minimum and maximum disk radii. The disk size-limits depend on the desired final target microstructure.

2.4 RVE Boundary Condition

The concepts of a Representative Volume Element (RVE) and a Periodic Boundary Condition (PBC) are intrinsically linked. A two dimensional PBC is required: (i) *to constrain the motion of counterpart nodes on each pair of RVE boundaries to each other* and (ii) *to ensure stress continuity across boundaries*. To fulfil these conditions, the following constraints are applied on the boundaries of the RVE using the 'EQUATION' keyword option available in Abaqus™:

$$U_i^R = U_i^L + U_i^{d_i},\ U_i^T = U_i^B + U_i^{d_i},\ i = 1 \text{ to } 2 \tag{6}$$

$$U_i^R = U_i^L,\ U_i^T = U_i^B,\ i = 3 \tag{7}$$

where the superscripts L, R, T and B indicate the left, right, top and bottom boundaries, respectively. U is the nodal displacement in the i^{th} direction, the subscript, i, represents the degree of freedom with i = 1, 2 indicating displacements in the X (transverse) and Y (perpendicular) directions and i = 3 indicating rotation about an axis lying perpendicular to the X–Y plane. Equations (6) and (7) automatically lead to perpendicular RVE compression. Hence, to apply compressive loading in any other arbitrary direction the plane of reference must be rotated accordingly [Schmidt, 2004].

3. Microstructure Generation and Finite Element Method

3.1 Finite Element Computation

Throughout this investigation a constant relative density of ρ_R=0.05 is used. Hence, a constant element cross sectional area is maintained in all the finite element models of this investigation. The same procedure used in both Alsayednoor et al. (2013) and Zhu et al. (2001[a]) is applied to calculate the beam thickness, t, i.e.

$$t = \frac{\rho_R A}{\sum_{k=1}^{n} l_k} \tag{8}$$

here n is the number of elements, A is the area of the RVE and l is the length of each individual element. For all cases, the material model is linear elastic with a Young's modulus, E_S, of 1 GPa, a material density, ρ_m, of 2000 kg m^{-3} and a Poisson's ratio of 0.33 consequently it should be noted that all conclusions from this work are restricted to linear elastic behaviour of the constituent material. This is clearly a significant simplification compared to real foam materials undergoing large deformations, but one which allows the investigation to focus on the influence of microstructural morphology rather than material behaviour. In order to eliminate the effect of unrealistically short elements near the border of the RVE, resulting from the cropping operation, (see Figure 4) , elements with thickness-to-length ratio above 1/8 were deleted prior to using the RVE in the FE simulations. Periodicity between the two counterpart boundaries was preserved, by considering each small element as a point and adjusting counterpart boundary elements accordingly. A mesh sensitivity study was performed, varying the number of elements per strut from 1 to 10. Good convergence was found using 5 elements and so this number was adopted for all subsequent simulations reported in this investigation (Zhu and Windle, 2002 also used 5 elements per strut in their investigation). Timoshenko beam elements (B22 in the Abaqus library) were employed and the Abaqus™ Standard implicit solver was used . Contact between elements was not modelled as the maximum compressive strain applied to the RVEs was no more than 10%; results from Alsayednoor et al. (2013) suggested contact between elements only becomes important at compressive strains of around 30%.

3.2 Evaluation of RVEs

When creating RVEs using numerical algorithms, it is clearly desirable to generate realistic microstructural morphologies. But what constitutes a 'realistic microstructure'? Certain realistic microstructural properties are relatively straightforward to anticipate. For example, a foam showing an isotropic mechanical response is generally expected to have no statistical directional dependence within its microstructure, i.e. there should be no preferred direction of cell orientation [Benouali et al. 2005; Jebur et al. 2012]. Likewise, poly-dispersity of real foams (or the lack of it) is evident when examining real micro-CT data [Montminy et al. 2004; Benouali et al. 2005] and is seen to vary from one type of foam to the next. It is therefore desirable to develop numerical algorithms that can control the degree of poly-dispersity in the digital microstructure. Other measures of realism relating to a foam's microstructure are less obvious. Referring to Figure 3, comparison with micro-CT images [Jebur, 2013] suggests that Figure 3b is more realistic than Figure 3a. Cells in Figure 3a are rather angular; a morphology unlikely to occur in a real gas-expanded foam due to minimisation of the energy associated with free surfaces (related to the second law of thermodynamics) [Jang et al. 2010]. Various statistical measures can be used to analyse the realism of the cell morphology, including the number of struts per cell and the strut intersection angles [Montminy et al. 2004; Kraynik, 2006]. In this section, the goal is to scrutinise each aspect of the digital microstructures and evaluate the performance of each of the three numerical methods discussed in Section 2. In each case, the mechanical response of the RVEs is examined and results of the morphological and mechanical analyses are compared. A simple and effective way to examine the mechanical anisotropy of the various RVEs is to apply uniaxial compressive loads along different directions with respect to the orientation of the RVE. Note that the response to alternative loading cases is also of interest, and indeed would be necessary if the RVEs were to be used to accurately determine the parameters of macro-scale constitutive models (e.g. hyperelastic models). Nevertheless, such loading cases are beyond the requirements of the current investigation and so are deferred to future work.

3.2.1 Evaluation of Microstructure Generated using the Basic Voronoi Tessellation

To study the possible relationship between the degree of irregularity and morphological / mechanical anisotropy of microstructures generated using basic Voronoi tessellation (see Section 2.1), four different values of α have been employed (α = 5, 15, 25 and 50). To obtain useful representative results using an RVE-based study, one must use either an RVE containing enough information (i.e. a large enough number of cells), or alternatively perform enough repeat simulations using smaller RVEs, to provide reliable representative results. Alsayednoor et al. (2013) demonstrated that the second strategy is the more computationally efficient approach and so for each degree of irregularity, 20 random RVEs with periodic boundary and boundary conditions, each containing 550 cells have been generated. Examples are shown in Figure 5.

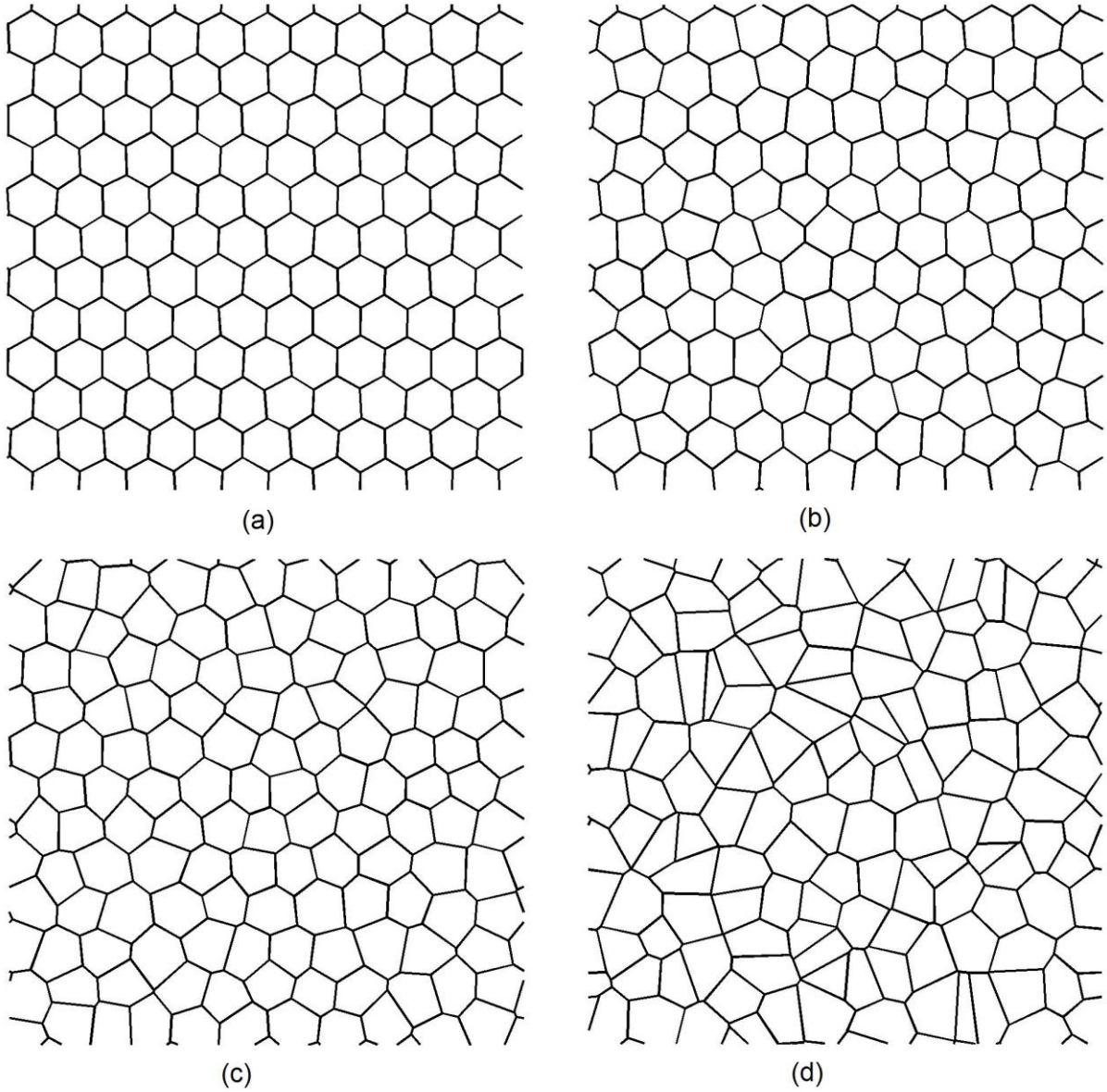

Figure 5: RVEs with 6 different degree of irregularity (a) α = 5, (b) α = 15, (c) α = 25, (d) α = 50

Algorithms were written to automatically generate statistical data from all 20 RVEs used for each case. Techniques used by these algorithms are described in [Alsayednoor, 2013]. Typical statistical data relating to cell orientation and size, generated from RVEs similar to the examples shown in Figure 5 are provided in Figures 6 to 9. A variety of statistical measures can be analysed [Alsayednoor, 2013; Montminy et al. 2004; Kraynik, 2006], for brevity, this investigation is limited to cell orientation, normalised size distribution, the number of struts per cell and the strut internal intersection angle. All RVE simulations in this investigation have a side

length of 1mm. Then, based on the area of single regular hexagonal cell, the all cellular areas were normalised.

In Figure 6, each black point represents an individual cell. The location of the point in the figure indicates both the area of the individual cell and its orientation. Radial distance from the origin indicates the area of the cell while the polar location of the point indicates cell orientation. The radius of the red circle represents the average cell size within the RVE. Figure 6, shows that for RVEs with very slight irregularity (α = 5) almost all the cells are orientated close to the angles 30^o, 90^o and 150^o. This is to be expected as the structure is close to that of a regular honeycomb. The area of the individual cells is almost constant, i.e. mono-disperse, as indicated by the fact that most of the points lie close to the red semi-circle. As the degree of irregularity increases from 5 to 50 the data becomes progressively more scattered around those angles and the points show increasing scatter away from the red semi-circle, indicating that the cell microstructure becomes increasingly poly-disperse as irregularity increases.

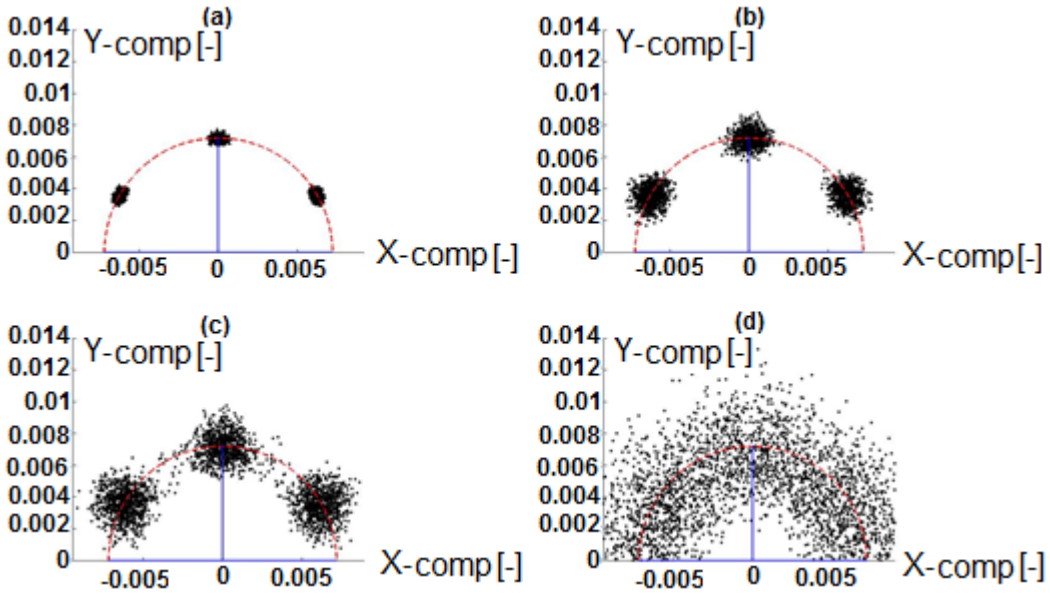

Figure 6: Polar representation of cellular orientation. The X and Y axis represent the length of the normalised components of the semi-major axis of an ellipse, fitted within each individual cell of the RVE, multiplied by the cell's area (black dots). The results are for microstructures generated using a basic Voronoi tessellation algorithm. (a) α=5, (b) α=15, (c) α=25, (d) α =50. The radius of the red circle represents an average value of the data for a given RVE

This can also be seen in Figure 7, which shows a histogram of cell area for each degree of irregularity. The histogram distributions become broader as the degree of

irregularity increases. A truly isotropic RVE should have no preferred directional orientation in the microstructure, i.e. in terms of Figure 6, there should be no concentration of the points in any particular direction. By increasing the degree of irregularity, α, the cellular orientations tend to become less concentrated in any particular direction and the RVE morphology tends to become more random and isotropic. Figure 5 clearly shows that the cost of this isotropy is a less realistic microstructure with individual cells taking a less realistic, more angular form.

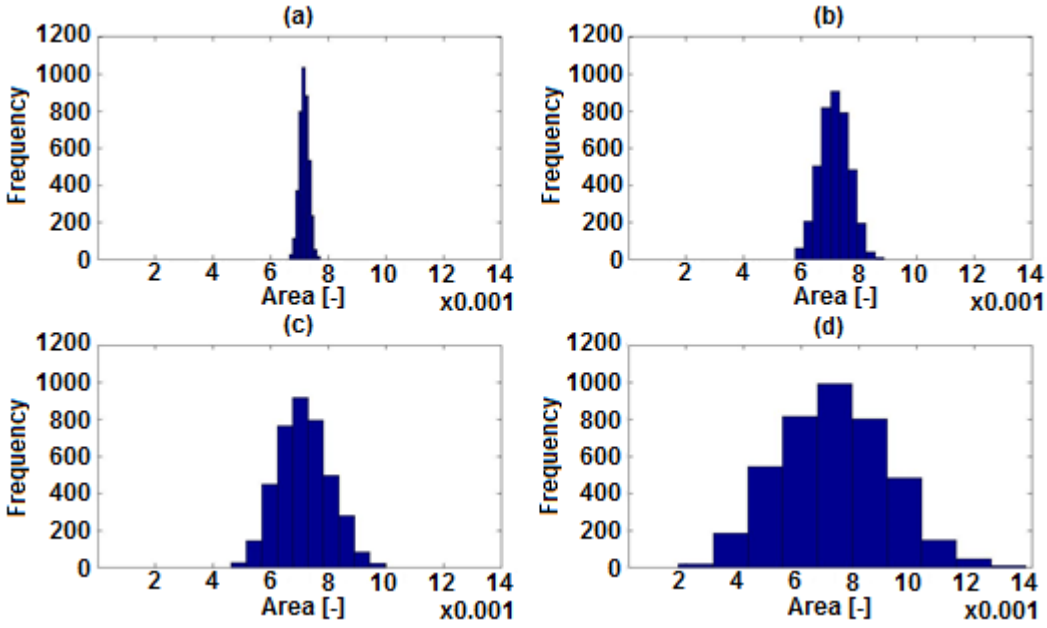

Figure 7: histogram of cellular area for undeformed state of microstructure generated from Basic Voronoi Tessellation. (a) α=5, (b) α=15, (c) α=25, (d) α =50.

Histograms showing the number of struts per cell and the strut internal intersection angle are plotted in Figures 8 and 9 and are an effective way to quantify the realism of average cell morphology. For a low degree of irregularity, the microstructure remains similar to that of a hexagonal honeycomb and all cells contain 6 struts (see Figure 8a). As might be expected, the strut internal intersection angle remains close to 120 degrees. For high degrees of irregularity some cells containing 5 and 7 struts (α = 25) and even as few as 4 and as many as 9 struts (α = 50) are generated (see Figure 8c and 8d). If these were regular cells, one may expect to see strut internal intersection angles as low as 108^o and as high as 129^o when α = 25 and as low as 90^o and as high as 140^o when α = 50. Examination of Figure 9c and 9d, reveals a much wider range of strut internal intersection angles; lower than 65^o and higher than 160^o when α = 25 and lower than 28^o and higher than 177^o when α = 50, this

exaggerated range in internal intersection angles is a good indicator of the highly irregular and angular cell shapes shown in Figure 5c and 5d.

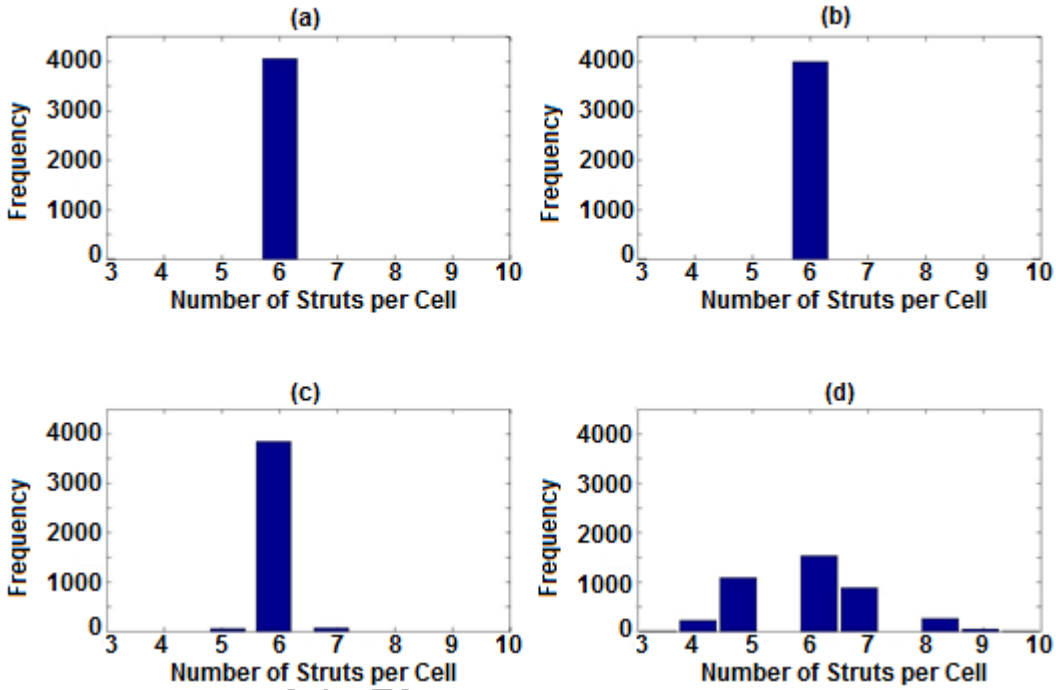

Figure 8: histograms for number of struts within each cell for undeformed state of microstructure for different degrees of irregularity**:** (a) α=5, (b) α=15, (c) α=25, (d) α=50

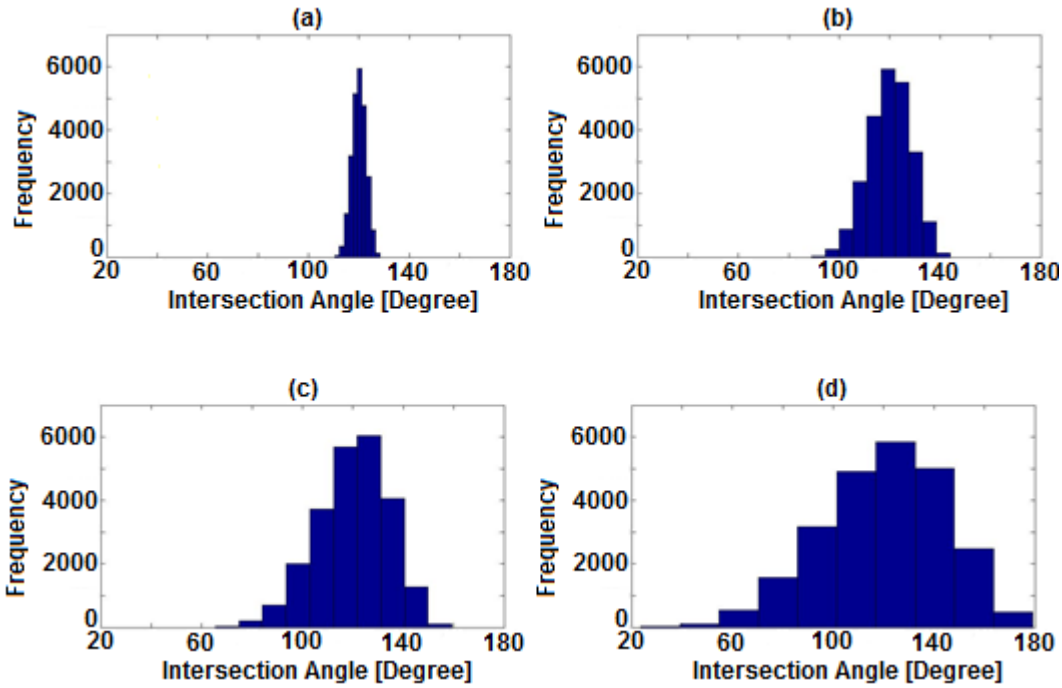

Figure 9: histograms for strut intersection angle within each cell for undeformed microstructures using different degrees of irregularity**:** (a) α=5, (b) α=15, (c) α=25, (d) α=50

To examine the mechanical response, the RVEs were subject to 10% compression in the vertical direction, horizontal and at 45^{o} directions. The results are shown in Figure 10. At very low strains (<2% compression) the stiffness response in the three directions is practically identical for any of the three directions. Given that analytical theory predicts an isotropic response for honeycomb structures compressed under small strains [Gibson and Ashby, 1997], this result is to be expected. At larger strains (>2% compression), the results diverge for low degrees of irregularity, reflecting an anisotropic stiffness response of a regular honeycomb structure under large strain compression [Zhu et al. 2006]. Increasing the degree of irregularity clearly leads to a more isotropic response at large strains, reflecting the increasingly isotropic morphology observed in the randomised microstructure, as indicated in Figure 6. It is worth noting that the small strain stiffness of the RVEs tends to increase with increasing degree of irregularity (for α=5, 15, 25 and 50 the moduli are: 171.66±1.15, 175.00±2.65, 186.00±1 and 238.33±6.35 KPa respectively), a result in agreement with that found previously by Zhu et al. 2001[a].

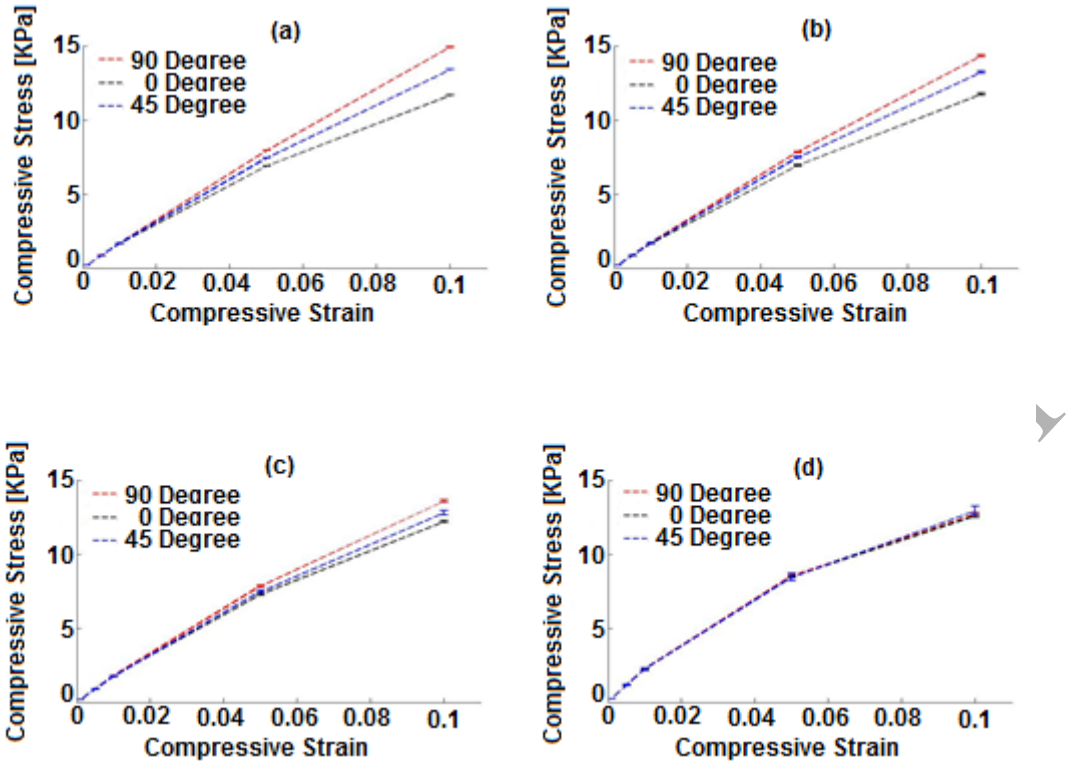

Figure 10: Averaged stress-strain curves for compressed RVEs generated fusing basic Voronoi Tessellation and with degree of irregularity: (a) α=5, (b) α=15, (c) α=25, (d) α=50

3.2.2 Evaluation of Microstructure Generated using the Centroidal Voronoi Tessellation Method

As discussed in Section 2.2, the Centroidal Voronoi Tessellation method used here employs the Lloyds algorithm to relax the microstructures originally generated using the basic Voronoi technique (see Section 2.1). To demonstrate the method, the maximum degree of irregularity, α = 50 (also known as Poisson Voronoi [Muche, 2005]), was used to create the RVEs. Once again 20 RVEs, each with periodic microstructure and boundary conditions, were generated. The microstructure was then 'relaxed' via application of the Lloyds algorithm (see, for example, Figure 3); there is an obvious visual change in the morphology of the relaxed microstructure with cells clearly less angular and of lower poly-dispersity than the microstructure prior to application of the Lloyds algorithm. Figure 11 is an equivalent polar plot to Figure 6 and shows that the relaxed microstructure is isotropic and the cell size distribution is rather mono-disperse. Comparison of Figure 12 and Figure 7d confirms the reduction of poly-dispersity after application of the Lloyd's algorithm. Figure 13 shows that the relaxed microstructure almost does not contain cells with

sides less than 5 and more than 7, indicating that the relaxation process does change the distribution for the number of struts within each cell. Nevertheless, Figure 14 reveals a range of strut internal intersection angles of between 95^o to 130^o; much closer to the range of 108^o and 129^o expected for regular pentagonal and heptagonal cells and much lower than the range of about 28^o to 177^o associated with the microstructure prior to relaxation.

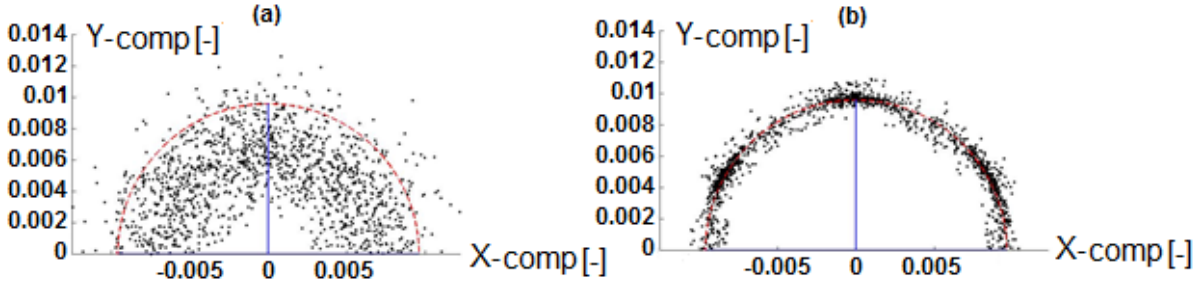

Figure 11: Polar representation of cellular orientation. The X and Y axis represent the length of the normalised components of the semi-major axis of an ellipse, fitted within each individual cell of the RVE, multiplied by the cell's area (black dots). The results are for microstructures generated using: (a) before Lloyd's relaxation, α=50 (b) after Lloyd's relaxation. The radius of the red circle represents an average value of the data for a given RVE

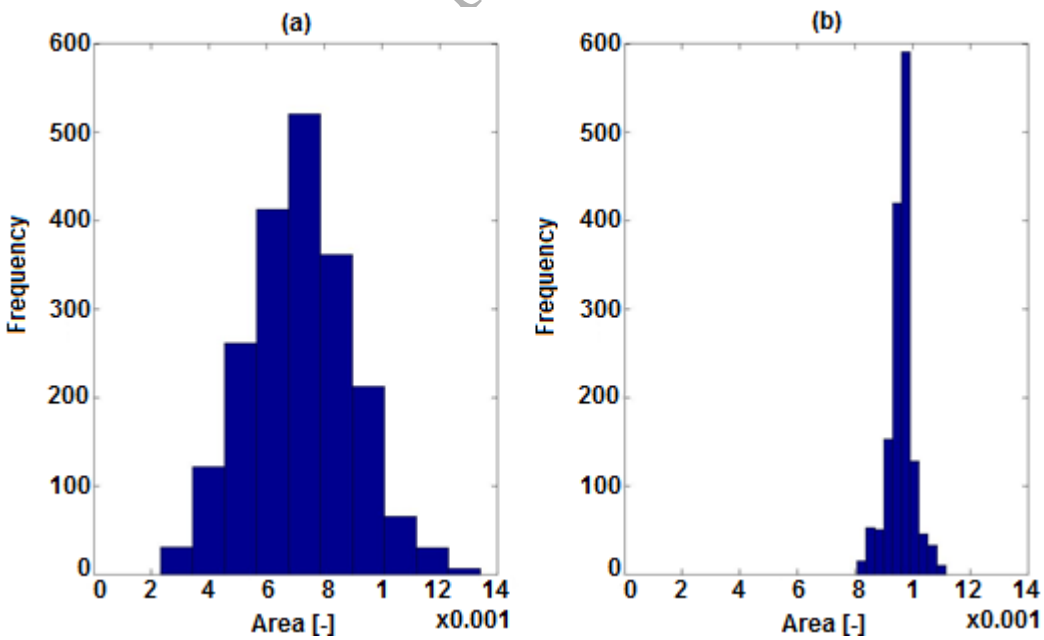

Figure 12: histograms of cellular area for microstructure: (a) before Lloyd's relaxation, α=50 and (b) after Lloyd's relaxation.

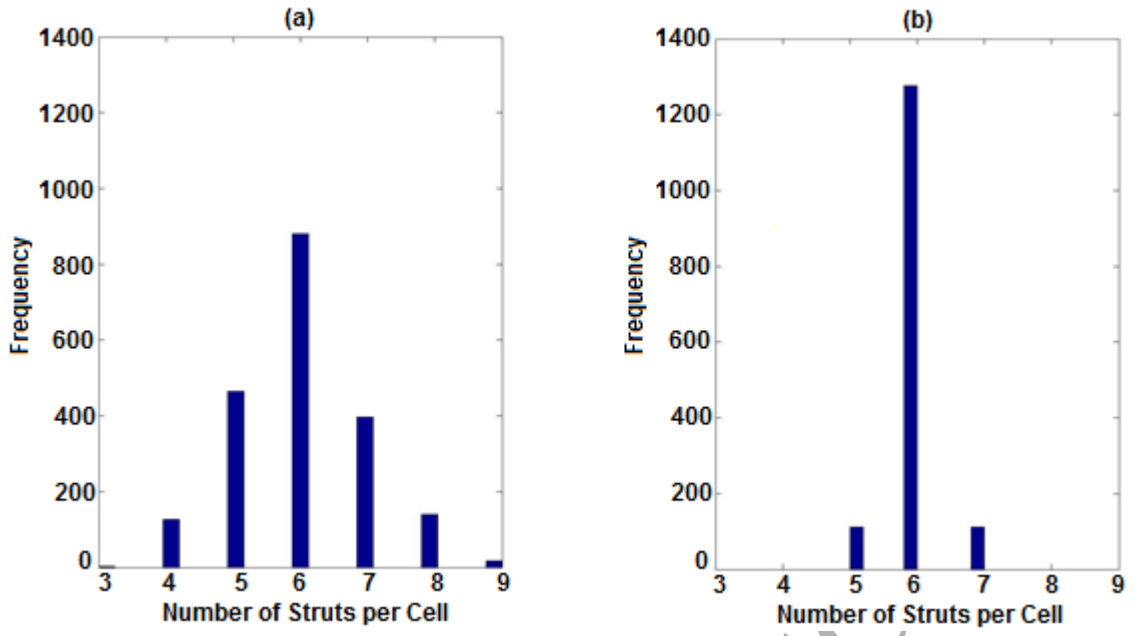

Figure13: histograms for number of struts within each cell for**:** (a) before Lloyd's relaxation, α=50 and (b) after Lloyd's relaxation

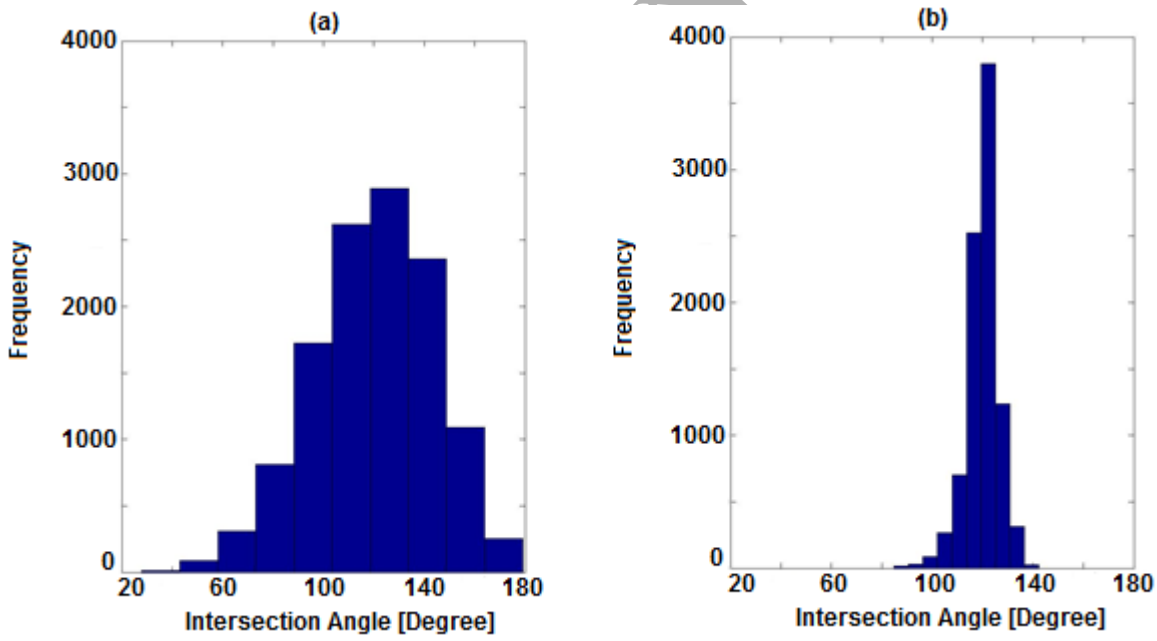

Figure14: histograms for struts intersection angle within each cell for: (a) before Lloyd's relaxation, α=50 (b) after Lloyd's relaxation

The relaxed RVEs were also subject to 10% compression in the vertical direction, horizontal and at 45^{o} directions. As expected, Figure 15 shows an isotropic mechanical response. The stiffness is lower than that of the fully randomised microstructure from which it is generated (189 +/-1.08 KPa after relaxation compared

to 238.33 +/-6.35 KPa prior to relaxation from a microstructure generated with α =50) and shows a more linear stress versus strain curve. It can be concluded that the CVT method can be applied to fully randomised RVEs (created using the basic Voronoi method) to generate isotropic RVEs with a realistic, predominantly mono-disperse microstructural morphology.

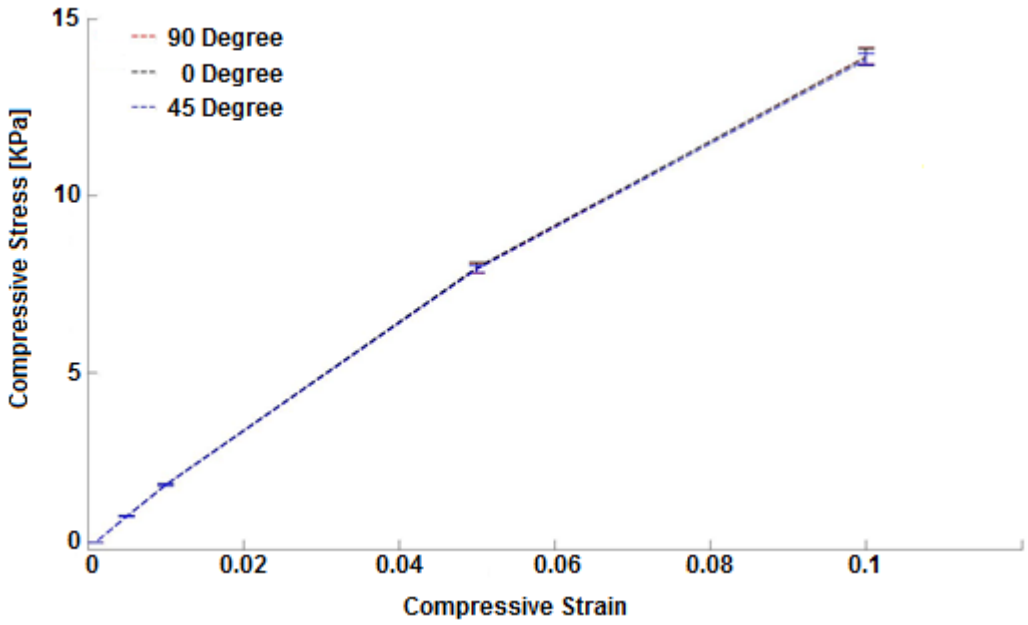

Figure 15: Averaged stress-strain curves for compressed RVEs generated using Lloyd's algorithm.

3.2.3 Evaluation of Microstructure Generated using the Laguerre-Voronoi Tessellation Method

To generate a dense packing of circular hard disks using the Drop and Roll method (see Section 2.3), a square with size 80X80 is considered (see supplementary materials for detailed explanation of the Drop and Roll algorithm). The following parameter values are used in Equation 5; r_{min} = 0.5, r_{max} = 5, m = 2.5, γ = [0.05, 0.1, 0.15, 0.20]. Increasing γ results in a higher poly-dispersity of the hard disc diameters, this is clearly reflected in the microstructural morphology shown in Figure 16. To evaluate the average behaviour for each degree of poly-dispersity, 20 RVEs were generated for each value of γ. All RVEs generated in this part of the study have the same relative density as RVEs generated using the alternative generation algorithms discussed in Sections 3.2.1 & 3.2.2. This was done in order to facilitate comparison of the average small strain compressive modulus of the different RVEs.

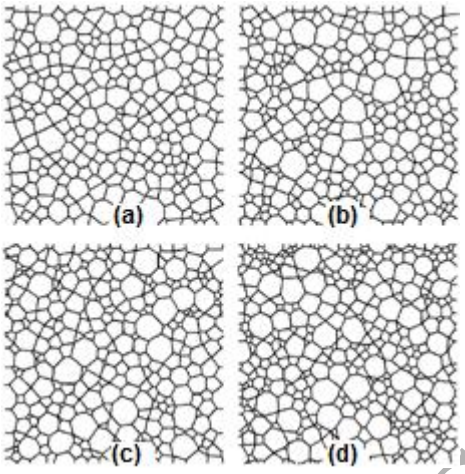

Figure 16: RVEs with 4 different degree of poly-dispersity: (a) γ=0.05, (b) γ=0.10, (c) γ=0.15, (d) γ=0.20. The final beam-based structures are obtained by solving the Apollonius problem [Wolfram Mathematica®] for packed hard circular disks and then by applying a Laguerre-Voronoi tessellation.

Examining the microstructural morphology in more detail, Figure 17 shows no obvious preferred direction for all cases and a high scatter of cell areas. The high poly-dispersity is confirmed in the histogram of Figure 18, which reveals how the distribution range increases with increasing γ, i.e. the poly-dispersity increases with increasing γ. Figure 18 shows that the shape of the distribution of cell areas is very different to that shown in Figures 7 and 12, and can be well-fitted using a log-normal distribution. This is to be expected given that the same type of function was used to generate the seeding discs using the Drop and Roll method. As γ increases, the probability of generating smaller cells is seen to increase. This can also be seen in Figure 17 which shows a denser clustering of points within the red circle at higher values of γ and a shrinking of the radius of the circle.

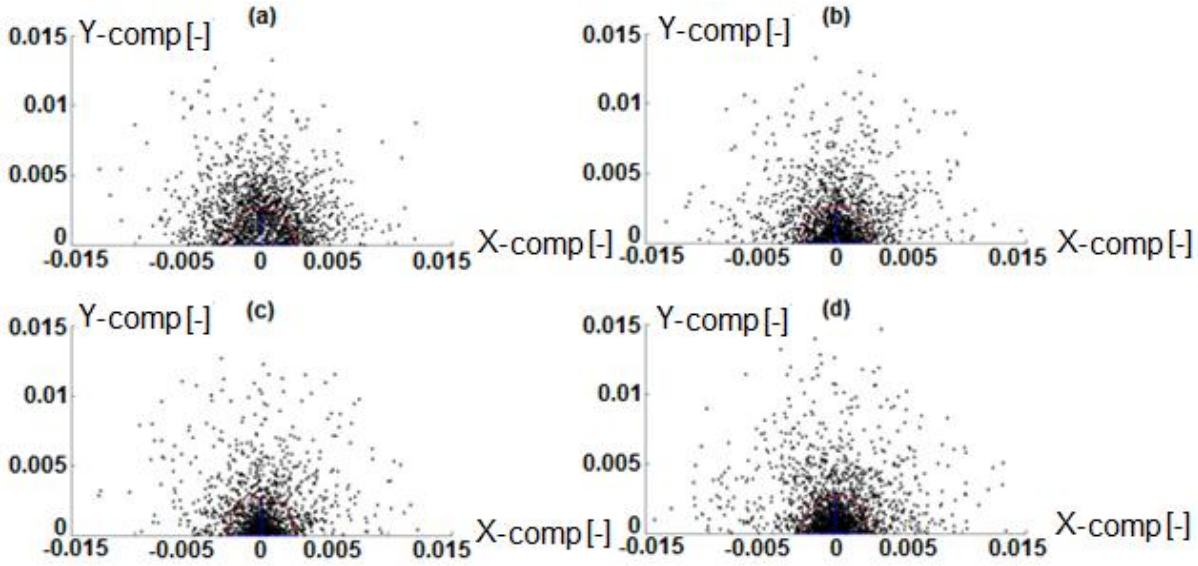

Figure 17: Polar representation of cellular orientation. The X and Y axis represent the length of the normalised components of the semi-major axis of an ellipse, fitted within each individual cell of the RVE, multiplied by the cell's area (black dots). The results are for microstructures generated using Laguerre-Voronoi Tessellation. (a) γ=0.05, (b) γ=0.10, (c), γ=0.15, (d) γ=0.20. The radius of the red circle represents an average value of the data for a given RVE

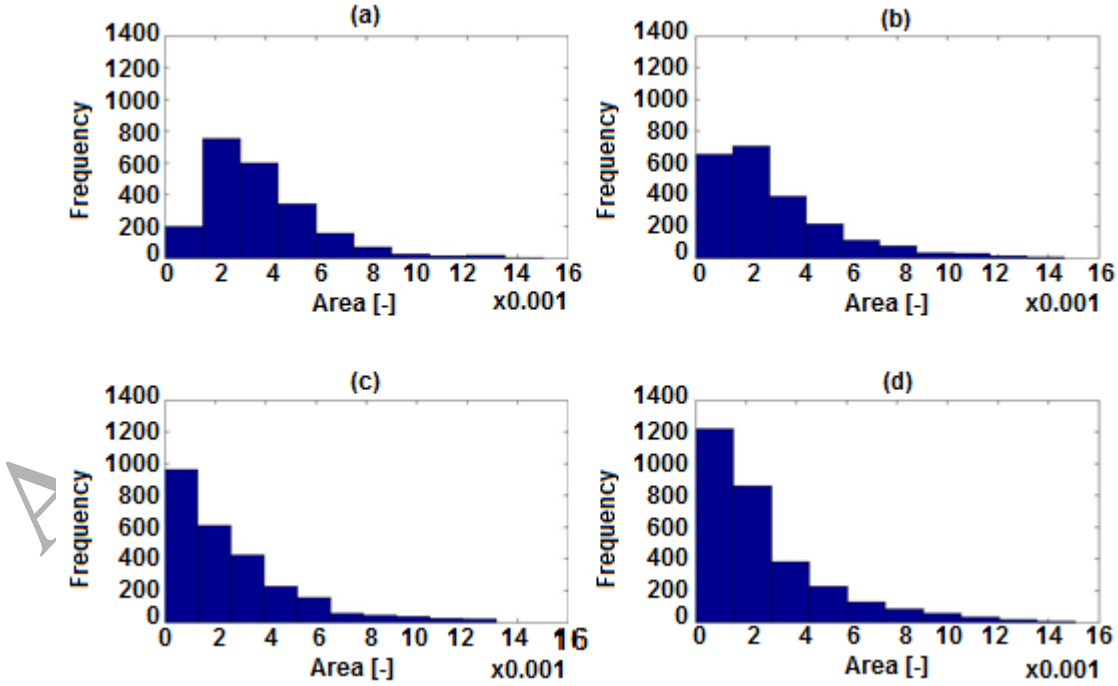

Figure 18: histograms of cellular area for undeformed state of microstructure generated from Laguerre-Voronoi Tessellation. (a) γ=0.05, (b) γ=0.10, (c), γ=0.15, (d) γ=0.20.

The resulting RVEs are also subject to 10% compression in the perpendicular (along Y-axis), transverse (along X-axis) and orthotropic directions (45^o rotated from X-axis). Figure 20 reveals that a small amount of anisotropy is evident in the mechanical response of the RVEs; the response in the 45^o direction is slightly stiffer than in the X or Y directions. The origin of this anisotropy stems from anisotropy induced in the microstructure due to the basic functioning of the modified Drop and Roll algorithm implemented in this investigation. A full discussion of the latter is provided in the supplementary material. Nevertheless, the anisotropy is much smaller than that resulting from the basic Voronoi algorithm (see Section 3.2.1). There is a slight trend towards increasing stiffness with increasing degree of poly-dispersity (for γ=0.05, 0.10, 0.15 and 0.20 the modulus calculated at 0.1% strain were: 197.38±25.9, 219.72±38.9, 206.23±18.43 and 233.78±45.55 KPa, respectively), in agreement with results by previous researchers [Fazekas et al. 2002]. This range of stiffness values lies within that found using the basic Voronoi algorithm, see Section 3.2.1.

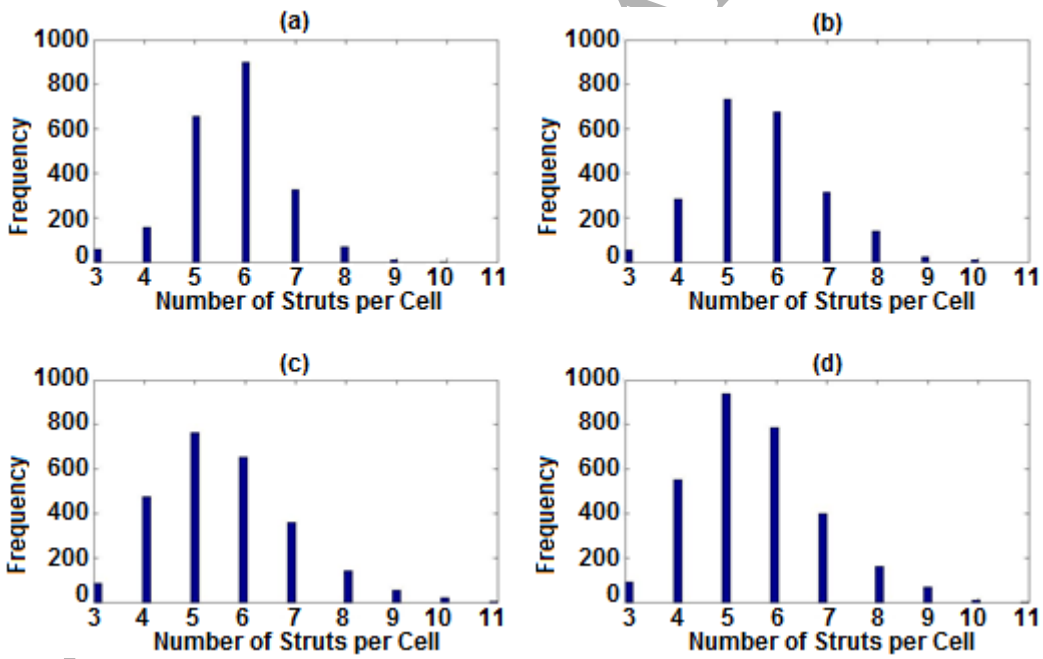

Figure 19: histograms for number of struts within each cell for undeformed state of microstructure for different degrees of of poly-dispersity: (a) γ =0.05, (b) γ =0.10, (c) γ =0.15, (d) γ =0.20

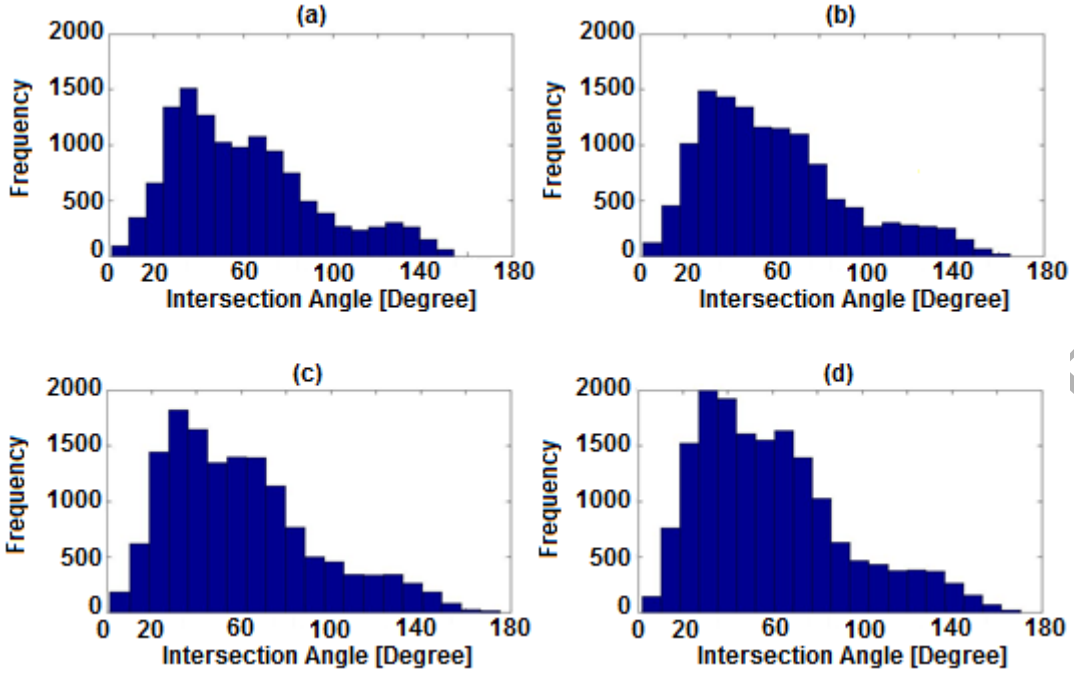

Figure 20: histograms for struts intersection angle within each cell for the undeformed microstructure generated using different degrees of of poly-dispersity: (a) γ =0.05, (b) γ =0.10, (c) γ =0.15, (d) γ =0.20

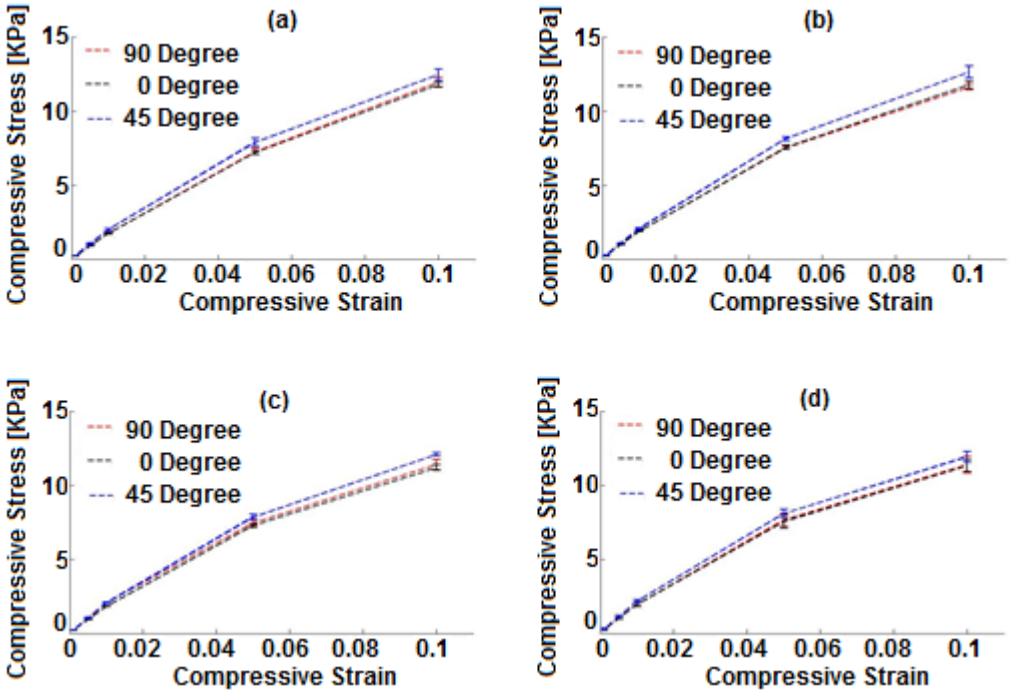

Figure 21: Averaged stress-strain curves for compressed RVEs generated from Laguerre-Voronoi Tessellation with degree of poly-dispersity: (a) γ =0.05, (b) γ =0.10, (c) γ =0.15, (d) γ =0.20

5. Conclusions

Various generation algorithms for 2-D foam-like RVE microstructures have been examined. The aim of the investigation was to evaluate the capabilities of these algorithms in generating realistic microstructures suitable for modelling the mechanical response of 2-D foams with fully random microstructures. While actual foams may in some cases possess transversely isotropic mechanical properties, a pre-requisite of microstructure generation algorithms should be the ability to produce mechanically isotropic RVEs; introduction of any intended anisotropy is subsequently a simple matter that can be achieved by simple affine stretching of the RVE microstructure.

The basic Voronoi tessellation method has been shown to generate microstructures possessing anisotropy; an unintended artefact of the seeding method used by the algorithm. A novel method of examining the microstructural morphology has been introduced using polar plots; these diagrams are a simple technique to visually highlight the statistical orientation and size distribution of cells within the RVEs. Mechanical compression tests conducted in three different directions on the RVEs confirmed the anisotropy revealed by the polar plots. It was found that morphological and mechanical anisotropy could be erased in RVEs with very high degrees of irregularity, though this created highly angular cell morphologies that were considered to be unrealistic. This effect has been studied by examining the strut internal angle distribution; an overly wide distribution is linked to an unrealistic, highly angular cellular morphology. Nevertheless, it has been shown that isotropic RVEs with realistic cellular morphologies can be created from such RVEs by applying a Centroidal Voronoi Tessellation algorithm to relax the microstructure. This combined approach results in the successful creation of isotropic mono-disperse RVEs, though the method is restricted to the generation of relatively mono-disperse microstructures. In order to generate poly-disperse microstructures the so-called Laguerre-Voronoi tesselation algorithm has been employed and combined with a modified version of the Drop-and-Roll method in order to create the seeding for the cells. The method is shown to successfully produce almost fully isotropic RVEs with a controlled degree of poly-dispersity. Together, the numerical algorithms analysed in this investigation offer the possibility to generate isotropic 2-D RVEs with realistic microstructures ranging from mono-disperse to highly poly-disperse cellular

morphologies. The small strain response of such RVEs is known to be reasonably well-predicted using analytical theory [Gibson and Ashby, 1997] and so the main value of type of RVEs presented in this paper would ultimately be exploited when simulating their large-strain mechanical response [e.g. Alsayednoor 2013].The main restriction of the current investigation is its focus on 2-D RVEs. A longer term goal is therefore to extend the techniques developed in this work, to the generation of equivalent 3-D RVEs, a more challenging task but ultimately more useful in modelling real foam materials.

Acknowledgements

The author's gratefully acknowledge funding from an EPSRC Doctoral Training Award (ref: EP/P504937/1) and EPSRC Frontier Engineering Awards (EP/K03877X/1).

References

ADAMCZYK, Z., SIWEK, B., ZEMBALA, M. & WERONSKI, P. 1997. Influence of polydispersity on random sequential adsorption of spherical particles. Journal of Colloid and Interface Science, 185, 236-244.

ALDERSON, A., RASBURN, J., AMEER-BEG, S., MULLARKEY, P. G., PERRIE, W. & EVANS, K. E. 2000. An auxetic filter: A tuneable filter displaying enhanced size selectivity or defouling properties. Industrial & Engineering Chemistry Research, 39, 654-665.

ALSAYEDNOOR, J., Modelling and characterisation of porous materials, PhD thesis, 2013

ALSAYEDNOOR, J., HARRISON, P. & GUO, Z. 2013. Large strain compressive response of 2-D periodic representative volume element for random foam microstructures. Mechanics of Materials, 66, 7-20.

ANTHOINE, A. 1995. Derivation of the Inplane Elastic Characteristics of Masonry through Homogenization Theory. International Journal of Solids and Structures, 32, 137-&.

AURENHAMMER, F. 1991. Voronoi Diagrams - a Survey of a Fundamental Geometric Data Structure. Computing Surveys, 23, 345-405.

AURENHAMMER, F. & KLEIN, R. "Voronoi Diagrams." Ch. 5 in Handbook of Computational Geometry (Ed. J.-R. Sack and J. Urrutia). Amsterdam, Netherlands: North-Holland, pp. 201-290, 2000

BANHART, J. 2001. Manufacture, characterisation and application of cellular metals and metal foams. Progress in Materials Science, 46, 559-U3.

BENOUALI, A. H., FROYEN, L., DILLARD, T., FOREST, S. & N'GUYEN, F. 2005. Investigation on the influence of cell shape anisotropy on the mechanical performance of closed cell aluminium foams using micro-computed tomography. Journal of Materials Science, 40, 5801-5811.

BOROVINSEK, M. & REN, Z. 2008. Computational modelling of irregular open-cell foam behaviour under impact loading. Materialwissenschaft Und Werkstofftechnik, 39, 114-120.

BOUIX, R., VIOT, P. & LATAILLADE, J. L. 2009. Polypropylene foam behaviour under dynamic loadings: Strain rate, density and microstructure effects. International Journal of Impact Engineering, 36, 329-342.

BRILLIANTOV, N. V., ANDRIENKO, Y. A., KRAPIVSKY, P. L. & KURTHS, J. 1998. Polydisperse adsorption: Pattern formation kinetics, fractal properties, and transition to order. Physical Review E, 58, 3530-3536.

CHEN, C., LU, T. J. & FLECK, N. A. 1999. Effect of imperfections on the yielding of two-dimensional foams. Journal of the Mechanics and Physics of Solids, 47, 2235-2272.

COOPER, D. W. 1988. Random-Sequential-Packing Simulations in 3 Dimensions for Spheres. Physical Review A, 38, 522-524.

DILLARD, T., N'GUYEN, F., MAIRE, E., SALVO, L., FOREST, S., BIENVENU, Y., BARTOUT, J. D., CROSET, M., DENDIEVEL, R. & CLOETENS, P. 2005. 3D quantitative image analysis of open-cell nickel foams under tension and compression loading using X-ray microtomography. Philosophical Magazine, 85, 2147-2175.

FAN, Z. G., WU, Y. G., ZHAO, X. H. & LU, Y. Z. 2004. Simulation of polycrystalline structure with Voronoi diagram in Laguerre geometry based on random closed packing of spheres. Computational Materials Science, 29, 301-308.

FARR, R. S. & GROOT, R. D. 2009. Close packing density of polydisperse hard spheres. Journal of Chemical Physics, 131.

FAZEKAS, A., DENDIEVEL, R., SALVO, L. & BRECHET, Y. 2002. Effect of microstructural topology upon the stiffness and strength of 2D cellular structures. International Journal of Mechanical Sciences, 44, 2047-2066.

GAN, Y. X., KAMLAH, M. & REIMANN, J. 2010. Computer simulation of packing structure in pebble beds. Fusion Engineering and Design, 85, 1782-1787.

GERVOIS, A., OGER, L., RICHARD, P. & TROADEC, J. P. 2002. Voronoi and radical tessellations of packings of spheres. Computational Science-Iccs 2002, Pt Iii, Proceedings, 2331, 95-104.

GIBSON, L.J., ASHBY, M.F., 1997. Cellular Solids – Structure and Properties.Cambridge University Press, Cambridge

GIBSON. L. N., Model of heterogeneous microscale in SOFI for Monte Carlo simulations, (2007), http://www.math.oregonstate.edu/~gibsonn/Teaching/MTH323-

001S09/Supplements/SamplePaper.pdf

GONG, L., KYRIAKIDES, S. & JANG, W. Y. 2005. Compressive response of open-cell foams. Part I: Morphology and elastic properties. International Journal of Solids and Structures, 42, 1355-1379.

GRAY, J. J., KLEIN, D. H., KORGEL, B. A. & BONNECAZE, R. T. 2001. Microstructure formation and kinetics in the random sequential adsorption of polydisperse tethered nanoparticles modeled as hard disks. Langmuir, 17, 2317-2328.

GRENESTEDT, J. L. & TANAKA, K. 1998. Influence of cell shape variations on elastic stiffness of closed cell cellular solids. Scripta Materialia, 40, 71-77.

GROSSE, J., DIETRICH, B., GARRIDO, G. I., HABISREUTHER, P., ZARZALIS, N., MARTIN, H., KIND, M. & KRAUSHAAR-CZARNETZKI, B. 2009. Morphological Characterization of Ceramic Sponges for Applications in Chemical Engineering. Industrial & Engineering Chemistry Research, 48, 10395-10401.

GUEDES, J. M. & KIKUCHI, N. 1990. Preprocessing and Postprocessing for Materials Based on the Homogenization Method with Adaptive Finite-Element Methods. Computer Methods in Applied Mechanics and Engineering, 83, 143-198.

GUO, Z. Y., SHI, X. H., CHEN, Y., CHEN, H. P., PENG, X. Q. & HARRISON, P. 2014. Mechanical modeling of incompressible particle-reinforced neo-Hookean composites based on numerical homogenization. Mechanics of Materials, 70, 1-17.

HARDENACKE, V. & HOHE, J. 2009. Local probabilistic homogenization of two-dimensional model foams accounting for micro structural disorder. International Journal of Solids and Structures, 46, 989-1006.

HARDER, J. M. & SILBERT, M. 1980. Binary Mixture of Hard-Spheres with Attractive Square-Well Interaction between Unlike Spheres. Chemical Physics Letters, 75, 571-574.

HE, D. & EKERE, N. N. 1998. Computer simulation of powder compaction of spherical particles. Journal of Materials Science Letters, 17, 1723-1725.

HILL, R. 1963. Elastic Properties of Reinforced Solids - Some Theoretical Principles. Journal of the Mechanics and Physics of Solids, 11, 357-372.

HOHE, J. & BECKER, W. 2003. Geometrically nonlinear stress-strain behavior of hyperelastic solid foams. Computational Materials Science, 28, 443-453.

HUBER, A. T. & GIBSON, L. J. 1988. Anisotropy of Foams. Journal of Materials Science, 23, 3031-3040.

JANG, W. Y., KRAYNIK, A. M. & KYRIAKIDES, S. 2008. On the microstructure of open-cell foams and its effect on elastic properties. International Journal of Solids and Structures, 45, 1845-1875.

JANG, W. Y., KYRIAKIDES, S. & KRAYNIK, A. M. 2010. On the compressive strength of open-cell metal foams with Kelvin and random cell structures. International Journal of Solids and Structures, 47, 2872-2883.

JEBUR, Q. H., HARRRISON, P., GUO, Z. Y., SCHUBERT, G. & NAVEZ, V. 2011. Characterisation and Modelling of a Melt-Extruded LDPE Closed Cell Foam. Advances in Experimental Mechanics Viii, 70, 105-110.

JEBUR, Q. H, Characterisation and modelling of transversely isotropic flexible viscoelastic foam, PhD thesis, 2013

JOHN, M. & LI, G. Q. 2010. Self-healing of sandwich structures with a grid stiffened shape memory polymer syntactic foam core. Smart Materials & Structures, 19.

KANAUN, S. & TKACHENKO, O. 2006. Mechanical properties of open cell foams: Simulations by Laguerre tesselation procedure. International Journal of Fracture, 140, 305-312.

KORNER, C., THIES, M. & SINGER, R. F. 2002. Modeling of metal foaming with Lattice Boltzmann automata. Advanced Engineering Materials, 4, 765-769.

KOUZNETSOVA, V., BREKELMANS, W. A. M. & BAAIJENS, F. P. T. 2001. An approach to micro-macro modeling of heterogeneous materials. Computational Mechanics, 27, 37-48.

KRAYNIK, A. M. 2006. The structure of random foam. Advanced Engineering Materials, 8, 900-906.

KRAYNIK, A. M., REINELT, D. A. & VAN SWOL, F. 2003. Structure of random monodisperse foam. Physical Review E, 67.

KRAYNIK, A. M., REINELT, D. A. & VAN SWOL, F. 2004. Structure of random foam. Physical Review Letters, 93.

LEFEBVRE, J., BASTIN, B., LE BRAS, M., DUQUESNE, S., PALEJA, R. & DELOBEL, R. 2005. Thermal stability and fire properties of conventional flexible polyurethane foam formulations. Polymer Degradation and Stability, 88, 28-34.

LI, K., GAO, X. L. & SUBHASH, G. 2006. Effects of cell shape and strut cross-sectional area variations on the elastic properties of three-dimensional open-cell foams. Journal of the Mechanics and Physics of Solids, 54, 783-806.

LIEBSCHER, A., PROPPE, C., REDENBACH, C. & SCHWARZER, D. 2013. Stochastic multiscale modeling of metal foams. Iutam Symposium on Multiscale Problems in Stochastic Mechanics, 6, 87-96.

LIM, D., KIM, H. S., KIM, Y. H., KIM, Y. H. & AL-HASSANI, S. T. S. 2008. Stress analysis of two-dimensional cellular materials with thick cell struts. Journal of Mechanical Science and Technology, 22, 835-845.

LIU, Y., WANG, W. P., LEVY, B., SUN, F., YAN, D. M., LU, L. & YANG, C. L. 2009. On Centroidal Voronoi Tessellation-Energy Smoothness and Fast Computation. Acm Transactions on Graphics, 28.

LLOYD, S. P. 1982. Least-Squares Quantization in Pcm. Ieee Transactions on Information Theory, 28, 129-137.

MAIRE, E., FAZEKAS, A., SALVO, L., DENDIEVEL, R., YOUSSEF, S., CLOETENS, P. & LETANG, J. M. 2003. X-ray tomography applied to the characterization of cellular materials. Related finite element modeling problems. Composites Science and Technology, 63, 2431-2443.

McCULLOUGH, K. Y. G., FLECK, N. A. & ASHBY, M. F. 1999. Uniaxial stress-strain behaviour of aluminium alloy foams. Acta Materialia, 47, 2323-2330.

MICHAILIDIS, N., STERGIOUDI, F., OMAR, H., PAPADOPOULOS, D. & TSIPAS, D. N. 2011. Experimental and FEM analysis of the material response of porous metals imposed to mechanical loading. Colloids and Surfaces a-Physicochemical and Engineering Aspects, 382, 124-131.

MIEHE, C. & KOCH, A. 2002. Computational micro-to-macro transitions of discretized microstructures undergoing small strains. Archive of Applied Mechanics, 72, 300-317.

MILLS, N. J. & ZHU, H. X. 1999. The high strain compression of closed-cell polymer foams. Journal of the Mechanics and Physics of Solids, 47, 669-695.

MILLS, N. J., Polymer Foams Handbook: Engineering and Biomechanics Applications and Design Guide, 2007, Butterworth-Heinemann

MONTMINY, M. D., TANNENBAUM, A. R. & MACOSKO, C. W. 2004. The 3D structure of real polymer foams. Journal of Colloid and Interface Science, 280, 202-211.

MUCHE, L. 2005. The Poisson-Voronoi tessellation: Relationships for edges. Advances in Applied Probability, 37, 279-296.

OKUBO, T. & ODAGAKI, T. 2004. Random packing of binary hard discs. Journal of Physics-Condensed Matter, 16, 6651-6659.

PATRICK, J. F., SOTTOS, N. R. & WHITE, S. R. 2012. Microvascular based self-healing polymeric foam. Polymer, 53, 4231-4240.

RAJ, S. V., KERR, J. A., NASA/TM-2010-216342/REV1, Glenn Research Center, Cleveland, OH (2010)

REYES, G. 2008. Static and low velocity impact behavior of composite sandwich panels with an aluminum foam core. Journal of Composite Materials, 42, 1659-1670.

RICHARD, P., OGER, L., TROADEC, J. P. & GERVOIS, A. 2001. A model of binary assemblies of spheres. European Physical Journal E, 6, 295-303.

ROBERTS, A. P. & GARBOCZI, E. J. 2002. Computation of the linear elastic properties of random porous materials with a wide variety of microstructure.

Proceedings of the Royal Society a-Mathematical Physical and Engineering Sciences, 458, 1033-1054.

ROUAULT, Y. & ASSOULINE, S. 1998. Modeling the disordered dense phase in the packing of binary mixtures of spheres. Journal of Colloid and Interface Science, 204, 87-92.

SCHMIDT, I. 2004. Deformation induced elasto-plastic anisotropy in metal foams - modelling and simulation. International Journal of Solids and Structures, 41, 6759-6782.

SHAN, Z. H. & GOKHALE, A. M. 2001. Micromechanics of complex three-dimensional microstructures. Acta Materialia, 49, 2001-2015.

SHULMEISTER, V., VAN DER BURG, M. W. D., VAN DER GIESSEN, E. & MARISSEN, R. 1998. A numerical study of large deformations of low-density elastomeric open-cell foams. Mechanics of Materials, 30, 125-140.

SILVA, M. J. & GIBSON, L. J. 1997. The effects of non-periodic microstructure and defects on the compressive strength of two-dimensional cellular solids. International Journal of Mechanical Sciences, 39, 549-563.

SILVA, M. J., HAYES, W. C. & GIBSON, L. J. 1995. The Effects of Nonperiodic Microstructure on the Elastic Properties of 2-Dimensional Cellular Solids. International Journal of Mechanical Sciences, 37, 1161-1177.

SMIT, R. J. M., BREKELMANS, W. A. M. & MEIJER, H. E. H. 1998. Prediction of the mechanical behavior of nonlinear heterogeneous systems by multi-level finite element modeling. Computer Methods in Applied Mechanics and Engineering, 155, 181-192.

SWAN, C. C. 1994. Techniques for Stress-Controlled and Strain-Controlled Homogenization of Inelastic Periodic Composites. Computer Methods in Applied Mechanics and Engineering, 117, 249-267.

TAGARIELLI, V. L., DESHPANDE, V. S., FLECK, N. A. & CHEN, C. 2005. A constitutive model for transversely isotropic foams, and its application to the indentation of balsa wood. International Journal of Mechanical Sciences, 47, 666-686.

VANDERBURG, M. W. D., SHULMEISTER, V., VANDERGEISSEN, E. & MARISSEN, R. 1997. On the linear elastic properties of regular and random open-cell foam models. Journal of Cellular Plastics, 33, 31-&.

VERHOOSEL, C. V., VAN ZWIETEN, G. J., VAN RIETBERGEN, B. & DE BORST, R. 2015. Image-based goal-oriented adaptive isogeometric analysis with application to the micro-mechanical modeling of trabecular bone. Computer Methods in Applied Mechanics and Engineering, 284, 138-164.

VISSCHER, W. M. & BOLSTERL.M 1972. Random Packing of Equal and Unequal Spheres in 2 and 3 Dimensions. Nature, 239, 504-&.

VORONOI, G., 1908. Nouvelles applications des parametres continus a la theorie des formes quadratiques. Journal fur Reine und Angewandte Mathematik 134, 198–312

WANG, B., WANG, R. X. & WU, Y. 2009. The Young's moduli prediction of random distributed short-fiber-reinforced polypropylene foams using finite element method. Science in China Series E-Technological Sciences, 52, 72-78.

WU, Y. G., FAN, Z. G. & LU, Y. Z. 2003. Bulk and interior packing densities of random close packing of hard spheres. Journal of Materials Science, 38, 2019-2025.

YOUSSEF, S., MAIRE, E. & GAERTNER, R. 2005. Finite element modelling of the actual structure of cellular materials determined by X-ray tomography. Acta Materialia, 53, 719-730.

ZHENG, Z. J., WANG, C. F., YU, J. L., REID, S. R. & HARRIGAN, J. J. 2014. Dynamic stress-strain states for metal foams using a 3D cellular model. Journal of the Mechanics and Physics of Solids, 72, 93-114.

ZHOU, J., HASSAN, M. Z., GUAN, Z. W. & CANTWELL, W. J. 2012. The low velocity impact response of foam-based sandwich panels. Composites Science and Technology, 72, 1781-1790.

ZHU, H. X., HOBDELL, J. R. & WINDLE, A. H. 2000. Effects of cell irregularity on the elastic properties of open-cell foams. Acta Materialia, 48, 4893-4900.

ZHU, H. X., HOBDELL, J. R. & WINDLE, A. H. 2001. Effects of cell irregularity on the elastic properties of 2D Voronoi honeycombs. Journal of the Mechanics and Physics of Solids, 49, 857-870.

ZHU, H. X., THORPE, S. M. & WINDLE, A. H. 2001. The geometrical properties of irregular two-dimensional Voronoi tessellations. Philosophical Magazine a-Physics of Condensed Matter Structure Defects and Mechanical Properties, 81, 2765-2783.

ZHU, H. X., THORPE, S. M. & WINDLE, A. H. 2006. The effect of cell irregularity on the high strain compression of 2D Voronoi honeycombs. International Journal of Solids and Structures, 43, 1061-1078.

ZHU, H. X. & WINDLE, A. H. 2002. Effects of cell irregularity on the high strain compression of open-cell foams. Acta Materialia, 50, 1041-1052.